Dissociative recombination of vibrationally excited HD^+: State-selective experimental investigation

Z. Amitay, A. Baer, M. Dahan, J. Levin, Z. Vager, and D. Zajfman
Department of Particle Physics, Weizmann Institute of Science, Rehovot 76100, Israel

L. Knoll, M. Lange, D. Schwalm, R. Wester, and A. Wolf
Max-Planck-Institut für Kernphysik and Physikalisches Institut der Universität Heidelberg, D-69029 Heidelberg, Germany

I. F. Schneider and A. Suzor-Weiner
Laboratoire de Photophysique Moléculaire, Université Paris XI, Orsay, France
(Received 1 June 1999)

The relative dissociative recombination rate coefficients for specific vibrational states of HD^+ have been measured. The method is based on using merged electron and molecular ion beams in a heavy-ion storage ring together with molecular fragment imaging techniques which allow us to probe the vibrational-state population of the stored beam as a function of time as well as the final state of the dissociation. The initial vibrational distribution of the stored ion beam (from a Penning ion source) is found to be in good agreement with a Franck-Condon model of electron impact ionization, apart from slightly larger experimental populations found for low vibrational states; its time evolution in the storage ring reflects the predicted vibrational level lifetimes. Dissociative recombination measurements were performed with the electron and ion beams at matched velocities (corresponding to average collision energies of about 10 meV), and at several well-defined collision energies in the range of 3–11 eV. The obtained vibrational-state specific recombination rate coefficients are compared with theoretical calculations and show that, although an overall agreement exists between experiment and theory, large discrepancies occur for certain vibrational states at low electron energy.
[S1050-2947(99)09411-1]

PACS number(s): 34.80.Gs

I. INTRODUCTION

A low energy collision between a molecular ion and a free electron often leads to recombination and subsequent dissociation of the molecular complex. For a diatomic molecular ion AB^+ initially in a vibrational level v and rotational state J, such a process, called dissociative recombination (DR), is schematically represented as

$$AB^+(v,J)+e^-(E)\rightarrow AB^{**} \rightarrow A(n)+B(n')(+E_k). \qquad (1)$$

In this reaction, the electron is captured by the molecular ion from the continuum, using up some of its relative kinetic energy E, and induces an initial electronic or rovibronic excitation of the molecular ion system, which (either directly or indirectly following the electron capture [1,2]) leads to an electronically doubly excited molecular compound AB^{**}. This state is unstable, and decays either by autoionization (the reverse process of recombination) or by dissociation into neutral fragments, completing the DR reaction. The dissociation yields fragments with considerable kinetic energy (E_k) and often also internal electronic excitation (characterized by the quantum numbers n and n'), depending on the energy balance of the reaction.

As an exothermic process occurring at a high rate, yielding products physically and chemically distinct from the original molecular ion, the DR reaction is of importance in many atmospheric, astrophysical, and laboratory plasma environments. To mention some examples, DR is the only significant electron removal process in the Earth ionosphere [3]. DR of O_2^+ in the ionospheres of Mars, Venus, and Earth is responsible for the green (5577 Å) and red (6300 Å) airglow emissions through the production of internally excited oxygen atoms which decay radiatively [2,4,5]. On Venus, the collision of H atoms with energetic O atoms produced by DR can result in the escape of the hydrogen from the atmosphere [6]. On Mars, DR of O_2^+ can provide sufficient energy to the product O atoms to allow them to escape the atmosphere [7], and in combination with the escape of hydrogen atoms it may be one of the mechanisms for the disappearance of water from the Martian surface [7]. Also the DR of N_2^+ is pertinent for the understanding of the anomalous isotopic ratio ^{15}N to ^{14}N on planet Mars [8,9]. This is due to the different kinetic energies given to the various N isotopes produced by the DR of $^{14}N^{14}N^+$ and $^{14}N^{15}N^+$ [10], which yield different escape probabilities for the fragments from the gravitational attraction. A prominent example in interstellar clouds is the production of water from the DR of H_3O^+ [11].

Despite the fact that DR has been studied extensively both theoretically and experimentally in a variety of methods and techniques, it is still not completely understood due to its complexity, and its effects in many environments are not well estimated. A very important aspect of this complexity is the high sensitivity of the DR process to the initial state of the molecular ion, and in particular to the *initial vibrational quantum state* v. This sensitivity shows up not only in the magnitude of the DR cross section and its dependence on the

electron energy E, but also as a change of the initial total energy available for dissociation. Hence it can have dramatic effects on the number of open channels for the various final atomic fragments and influence their final kinetic energy.

Quantitative understanding of the vibrational dependence of DR is important for many of the processes described above. For example, theoretical calculations have shown that the branching ratio for the different final states of the O fragments from the DR of O_2^+ is very sensitive to the initial vibrational excitation of O_2^+ [5,12–14]. Since it is known that molecular oxygen ions in the Earth thermosphere are produced in vibrational levels up to $v=7$ [15] by charge exchange of O^+ with O_2, this could change the ratio between the emission intensities of the airglow lines. For the DR of N_2^+ in the Martian atmosphere, the expected isotope differentiation between ^{15}N and ^{14}N is reduced considerably if the N_2^+ molecules are vibrationally excited, as compared to the situation with N_2^+ $(v=0)$ ions [8,10].

On the theoretical side, the effect of the initial vibrational state v of the molecular ion on the total DR rate coefficient enters via the initial vibrational wave function, and through the total energy of the molecular system in its center-of-mass frame of reference. In particular, calculations have shown that a very significant quantity for the capture of the electron is the Franck-Condon factor between the initial vibrational wave function $\Psi_{AB^+}(R,v)$ and the continuum vibrational wave function of the dissociative state $\Psi_{AB^{**}}(R,E_t)$ [2,14,16–18],

$$f(v,E_t)=\int \Psi^*_{AB^+}(R,v)\Psi_{AB^{**}}(R,E_t)dR. \qquad (2)$$

While the v dependence of Ψ_{AB^+} is obvious, also $\Psi_{AB^{**}}$ depends on v through the total energy E_t of the system, representing the sum of the initial vibrational energy of the molecular ion and the electron energy E. Moreover, the ''survival factor'' [1], describing the likelihood that the recombined intermediate state will decay via dissociation rather than by autoionization, also depends on the initial vibration. Here, an important role is played by the above $f(v,E_t)$ and similar Franck-Condon factors for the coupling between AB^{**} and other vibrational states (differing from the initial state v), which governs the autoionization rate of the molecular compound [2,14,16–18].

On the experimental side, the strong vibrational sensitivity of the DR process has been for many years one of the main obstacles for obtaining a reliable cross section which could be directly compared with theoretical calculations. The difficulties originate mainly from the inherent uncertainties in the knowledge of the initial vibrational excitation of the molecular ions upon their production in the ion source. Usually, molecular ions are produced by ionization of the parent neutral molecule, by dissociation and ionization of a neutral gas, or by two- and three-body (complex) collisions, and are in general created at very high vibrational excitation. During the past six years, heavy-ion storage rings have been used to produce intense and fast beams of molecular ions in their vibrational ground state [19]. In a storage ring, one can store many infrared active molecular ions for a time which is long enough to allow complete deexcitation via spontaneous radiative transitions of the unknown initial electronic and vibrational excitation. Rotational cooling has also been shown to occur, although over a much longer time scale [20,21].

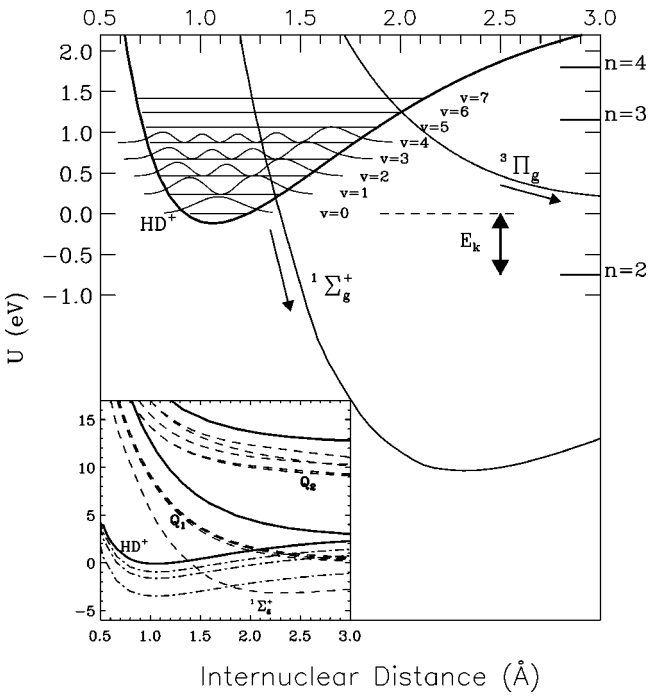

FIG. 1. Potential-energy curves for HD^+ and HD [33,43,45]. For HD^+ only the ground electronic state is shown together with the position of its vibrational levels and some corresponding vibrational wave functions squared. For HD, only some of the Q_1 and Q_2 states are shown.

Once the vibrationally cold $(v=0)$ molecular ions are prepared in the storage ring, their DR is measured by merging them with an intense electron beam in a collinear merged-beams configuration, allowing a very high resolution and a fine control over the collision energy. DR cross sections (or rate coefficients) of various important vibrationally cold molecular ions have been measured [19], and the inclusion of two- and three-dimensional molecular fragment imaging techniques has allowed for the identification of the final quantum states of the DR fragments as well as for measurements of the corresponding branching ratios [22–24]. These new experimental data have allowed detailed insights into the DR process of many molecular systems, including, for example, the identification of the active recombination mechanisms [23] and of the specific states which are involved in the recombination as well as in the dissociation phase.

Being the simplest molecular ions, H_2^+ and its infrared active isotopomer HD^+ are fundamental for the understanding of DR, serving as benchmarks for testing the various theoretical assumptions. HD^+ was chosen for many of these first experiments also because of the fact that it completely cools down radiatively to the $v=0$ state within a few hundred milliseconds storage time (the exact time depends on the initial population distribution).

For HD^+ ions initially in the ground electronic state $X^2\Sigma_g^+$ and the rovibrational state vJ, the DR process proceeds according to Eq. (1), as (see Fig. 1)

$$HD^+(X^2\Sigma_g^+,v,J)+e^-(E)\rightarrow HD^{**}$$
$$\rightarrow H(n)+D(n')(+E_k). \qquad (3)$$

For low-lying vibrational states and low-energy electrons, the dominant doubly excited dissociative state HD** is the $^1\Sigma_g^+$ state (Fig. 1). This state crosses all the vibrational levels of HD^+ (except for the $v=0$ state), and as such is an important recombination channel for all v. As the total energy E_t of the molecular system increases, either due to higher vibrational excitation or higher electron energy, additional energetically higher dissociative states, denoted as the Q_1 and Q_2 states (see Fig. 1) [33], become accessible and start playing a role. Eventually, at high total energy, they completely dominate the process.

As far as the DR of HD^+ in the ground vibrational state is concerned, the cross section has been measured over a wide range of electron energy at different storage rings [25–28]. Also the final states of the H and D atomic fragments have been determined as a function of electron energy, using molecular fragment imaging techniques [22,24]. At low electron energies, Rydberg resonances due to the so-called indirect recombination process have been observed. For vibrationally excited H_2^+, the cross section has been measured for an unknown distribution of vibrational states and very high values of the DR cross section have been observed, pointing out that the high vibrational states of H_2^+ (and consequently HD^+) should have very high recombination rate coefficients [29].

In general, the agreement of theoretical calculations with the experimental data of vibrationally cold molecular ions is rather good, although not always perfect both qualitatively and quantitatively [22,24,26–28]. However, for excited vibrational states, the situation is quite different, and even for the simplest molecular ion H_2^+ or its isotopomer HD^+, various calculations have yielded results disagreeing with each other (sometimes differing by more than an order of magnitude for specific vibrational states). The reasons for these large discrepancies are not clear, and the possibility that some basic aspects of the DR process are still undiscovered cannot be excluded.

In the following, we present a method, based on the storage ring technique, which allows us to extract the relative DR rate coefficients for specific vibrational states of the molecular ions. The present experiment is carried out on HD^+ and direct comparisons with theory both for low energy (thermal electron energy ~ 10 meV, initial vibrational states $v=0$–7) and high energy electrons (well-defined electron energies of $E=3$–11 eV, $v=0$–3) are presented. The low energy results given here have already been published in short form elsewhere [30]. The purpose of the present paper is to give a detailed discussion of the experimental technique, data analysis, and results.

II. EXPERIMENTAL PROCEDURE

A. Overview

In order to measure a state selective cross section, one often tries to produce the molecules in the desired vibrational state using laser techniques. Although these techniques are very powerful and do allow for an efficient transfer of population among the different initial states, they usually require a very special configuration of electronic (or rovibrational) states [31].

In the present experiment, we have chosen a different technique which is based on probing the vibrational population as a function of time, from the moment of injection into the storage ring up to complete vibrational relaxation, while at the same time, the DR cross section and/or the final-state branching ratios are measured. As will be shown later, this correlated measurement allows one to deduce DR information for specific single initial vibrational states which are populated at injection time.

The present experiment was conducted at the heavy-ion Test Storage Ring (TSR) located at the Max-Planck-Institut für Kernphysik, Heidelberg, Germany [32]. Through direct electron impact ionization of neutral HD molecules, a beam of HD^+ molecular ions was produced by a standard Penning ion source, accelerated to $E_i=2.0$ MeV using a Van-de-Graaff accelerator, and injected into the storage ring, where the ions were stored at this energy in the fields of bending and focusing magnets (see Fig. 2). After each injection, lasting for about 150 μs, typically 10^7 particles circulated in the ring (nominal circumference 55.4 m) in a vacuum of about 5×10^{-11} mbar with a mean storage lifetime of about 10 s. The experiment was composed of two main parts. On one hand, DR between the stored HD^+ ions and free electrons, supplied by the electron cooler, were measured by detecting the neutral fragments H and D downstream of the interaction region. On the other hand, under the same storage conditions, with the ions continuously circulating in the ring, a small part of the beam was extracted from the TSR toward a dedicated beam line, where the vibrational-state population was probed using the Coulomb explosion imaging (CEI) technique. Both the DR and the CEI measurements were conducted as a function of storage time, thus allowing their correlation.

B. Vibrational-state specific DR rate coefficients

At each turn and at all times starting from the injection, the circulating molecular ion beam was merged collinearly with the 3.5-cm-diameter electron beam of the electron cooler having a straight interaction region of 1.5 m length. The electron density had a typical value of 2×10^6 cm^{-3}. The electron and ion beam energies E_e and E_i (in the laboratory frame) determine the average relative motion between electrons and ions, which is characterized by the energy

$$E=[\sqrt{(m_e/m_i)E_i}-\sqrt{E_e}]^2, \tag{4}$$

where m_e and m_i denote the electron and the molecular ion mass, respectively. The energy E of average relative motion was varied by tuning the electron beam energy while keeping the energy of the stored ions at a fixed value. For the effective electron-ion collision energies also the velocity spreads in the merged beams must be considered; thus, at matched electron and ion beam velocities ($E=0$), the collision energies are dominated by the electron velocity distribution. In the comoving reference frame of the electron beam, the longitudinal electron temperature was $kT_\parallel\approx0.5$ meV and the transverse temperature $kT_\perp=10$ meV. Measurements were performed at $E=0$ and also at various energies E in the range of 3–11 eV. Under these latter conditions, the electron velocity spread resulted in a nearly symmetrical energy spread of 100–200 meV full width at half maximum

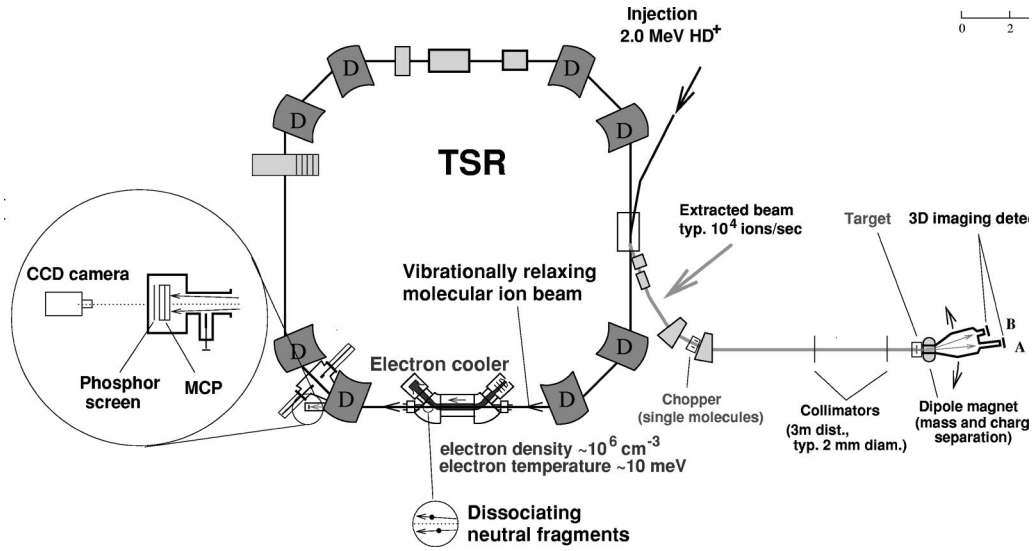

FIG. 2. Schematic drawing of the TSR storage ring, including the arrangement for measuring dissociative recombination rates and the extraction toward the dedicated beam line for Coulomb explosion imaging (CEI) of the molecular ions. The two CEI detectors are labeled by *A* and *B*; detector *A* was used for the H^+ and D^+ fragments in the present experiment.

(FWHM) around the average collision energy E. The influence of the ion velocity spread on the collision energies could always be neglected.

The DR rates were measured by detecting the neutral fragments H and D produced in the interaction region with the electrons, using a detector mounted straight ahead of the cooler at a distance of ~ 6 m from the center of the interaction region (see Fig. 2). Two different types of detectors were employed: a two-dimensional fragment imaging detector and a surface-barrier (energy sensitive) detector. Technical details related to the two-dimensional fragment imaging detector have been published previously [23].

The two-dimensional fragment imaging detector allows us to record, for a large number of recombination events, spectra of the transverse fragment distance, from which both the initial vibrational state v and the final asymptotic state nn' of the DR fragments can be determined. This provides a series of relative initial-to-final state-to-state DR rates as a function of storage time (i.e., as a function of the change in the vibrational distribution). Using the measured vibrational populations (see Sec. II C), these rates were converted to relative state-to-state rate coefficients. Because of the relatively high complexity of the imaging spectrum, which limits its resolution once too many DR channels are open, the imaging measurement was conducted only at zero relative electron energy ($E=0$). At higher collision energies ($E=3-11$ eV), the total DR rate was measured instead as a function of storage time employing the surface-barrier detector; combining this information with the measured time dependences of the vibrational populations, state-specific relative rate coefficients (summed over all final states) were obtained for several vibrational states.

1. State-to-state relative contributions in DR fragment spectra

For the low energy state-to-state relative rate-coefficient measurement, the H and D neutral DR fragments were detected by a two-dimensional (2D) fragment imaging detector [22,23]. In short, this detector is composed of an 80-mm-diameter Chevron microchannel plate (MCP) coupled to a phosphor screen. Each particle impact on the detector created a light spot of $\approx 1-1.5$-mm diameter on the phosphor screen, and the image of these spots was digitized using a CCD camera, coupled to a fast frame grabber device, which was read out by a computer. On analysis, the positions of the light spots were determined using a peak finding procedure, and for each frame that contained two spots their relative distance was deduced. The position resolution of the detector was ≈ 100 μm and the minimum distance which could be distinguished between two spots was ≈ 2 mm. The CCD camera was measuring at a constant rate of 50 frames per second, while the actual rate of DR events was of the order of a few kHz; therefore the detector was operated in the so-called ''trigger mode'' [23] which assured that only one DR event was recorded per frame.

The 2D projection onto the plane of the detector (perpendicular to the beam direction) of the 3D spatial relative distance between the DR fragments upon their arrival to the detector, measured event by event, yields an accumulated spectrum of projected distances. Under specific experimental conditions, the shape of this projected-distance spectrum is determined directly by the states involved in the DR process, and the analysis allows us to identify the different possible values for the kinetic energy release E_k of the DR fragments in the molecular frame of reference, together with their relative contributions to the spectrum. The underlying principle of the method being used here is that each such value of E_k is actually characteristic of events for a specific initial-to-final DR channel. For the recombination process as represented by Eq. (3) and illustrated in Fig. 1, the kinetic energy release E_k is given by energy conservation as

$$E_k = E_{vJ} + E - E_{nn'}, \tag{5}$$

where

$$E_{vJ} = E_v + J(J+1)B \tag{6}$$

is the initial rovibrational energy of the molecular ion, with E_v being the vibrational energy (corresponding to $J=0$) and B the rotational constant of the molecular ion. $E_{nn'}$ is the energy of the final asymptotic state nn' of the DR fragments. Since isotopic shifts are not resolved, events with final states nn' and $n'n$ are equivalent for this experiment. All energies are measured relative to the same energy level, which for convenience was chosen to be the ground rovibrational state $v=0,J=0$ of HD^+. Considering the average rotational energies of the stored HD^+ ions, as discussed below, the true collision energies of the DR events can be represented with sufficient accuracy by the average relative energy E of the merged beams, neglecting the influence of the electron and ion beam velocity spreads. Based on Eqs. (5) and (6), and for a fixed electron energy E, each kinetic energy value E_k can be directly correlated to an initial-to-final state-to-state DR channel $vJnn'$ from specific initial state vJ to specific final state nn'. The kinetic energy release in such a case will be denoted as $E^{(E)}_{k,vJnn'}$.

A single DR event of a molecular ion with laboratory energy E_i, taking place at a distance s from the detector with an angle θ between the internuclear axis and the beam direction at the time of dissociation, results in a projected distance D between the DR fragments in the plane of the detector given by

$$D=s\,\delta^{(E)}_{vJnn'}\sin\theta, \tag{7}$$

$$\delta^{(E)}_{vJnn'}=\frac{(m_{\mathrm{H}}+m_{\mathrm{D}})}{\sqrt{m_{\mathrm{H}}m_{\mathrm{D}}}}\sqrt{E^{(E)}_{k,vJnn'}/E_i}, \tag{8}$$

where m_{H} and m_{D} are the fragment masses. The upper index of δ indicates its dependence on the relative energy E through $E^{(E)}_{k,vJnn'}$ [cf. Eq. (5)]. Taking into account the fact that DR events occur along the whole interaction region with the electrons (ranging between distances s_1 and s_2 from the detector) with equal probability, and assuming an isotropic distribution of θ in the molecular frame of reference, which is good at least in the limit of vanishing collision energy, one gets for the normalized projected-distance distribution $P^{(E)}_{vJnn'}(D)$ the following line shape [23]:

$$P^{(E)}_{vJnn'}(D)=\begin{cases}\dfrac{1}{(s_2-s_1)\,\delta^{(E)}_{vJnn'}}\left(\arccos\dfrac{D}{s_2\delta^{(E)}_{vJnn'}}-\arccos\dfrac{D}{s_1\delta^{(E)}_{vJnn'}}\right) & \text{for } 0\leqslant D\leqslant s_1\delta^{(E)}_{vJnn'},\\ \dfrac{1}{(s_2-s_1)\,\delta^{(E)}_{vJnn'}}\arccos\dfrac{D}{s_2\delta^{(E)}_{vJnn'}} & \text{for } s_1\delta^{(E)}_{vJnn'}\leqslant D\leqslant s_2\delta^{(E)}_{vJnn'},\\ 0 \quad \text{otherwise.}\end{cases} \tag{9}$$

The line shape of Eq. (9) rises from zero at $D=0$ to a peak at distance $D=s_1\delta^{(E)}_{vJnn'}$, and then decreases again to zero with an edge at the maximal possible distance $D=s_2\delta^{(E)}_{vJnn'}$. For fixed E_i, s_1, and s_2, each DR channel $vJnn'$ is characterized by the specific line shape obtained for the kinetic energy release $E^{(E)}_{k,vJnn'}$ of this channel.

In general, several states are involved in the DR process, thus the total accumulated projected distance spectrum $P^{(E)}(D;t)$ measured at time t after injection is given by a summation over all energetically open DR channels $(E^{(E)}_{k,vJnn'}\geqslant 0)$:

$$P^{(E)}(D;t)=\sum_{vJnn'} q^{(E)}_{vJnn'}(t)P^{(E)}_{vJnn'}(D), \tag{10}$$

where the contributions (number of events) $q^{(E)}_{vJnn'}(t)$ of the different DR channels satisfy the relation

$$\frac{q^{(E)}_{vJnn'}(t)}{\sum_{vJnn'} q^{(E)}_{vJnn'}(t)}=\frac{r^{(E)}_{vJnn'}(t)}{\sum_{vJnn'} r^{(E)}_{vJnn'}(t)}. \tag{11}$$

Here $r^{(E)}_{vJnn'}(t)$ represents the partial DR rate at time t from the respective channel. The corresponding time-independent rate coefficient $\alpha_{vJnn'}(E)$ is related to $r^{(E)}_{vJnn'}(t)$ through

$$r^{(E)}_{vJnn'}(t)=K\alpha_{vJnn'}(E)N_{vJ}(t), \tag{12}$$

where $N_{vJ}(t)$ stands for the number of ions in the stored beam populating the rovibrational state vJ at time t after injection, and K is a normalization constant independent of E, $vJnn'$, and t.

As pointed out above, complete vibrational cooling of HD^+ is achieved after storage for about 300 ms. However, such time is too short for rotational cooling, as pure rotational relaxation would require storage times longer by orders of magnitude [21]. Thus, it is reasonable to assume that the rotational population stays constant during the whole time interval of our measurement (i.e., over the first $\sim$400 ms of storage), and is identical to the initial rotational population of the ion source. The production of the HD^+ ions by direct electron impact ionization of HD is not expected to change much the initial rotational population distribution of the parent HD molecules [34,35]. Such population is characterized by a Boltzmann distribution with a temperature between a few hundred degrees K up to about 1000 K. In the stored molecular ions, small deviations from the initial distribution will occur due to rovibrational transi-

tions where the J quantum number changes as determined by the selection rules [36]; however, the experimental results obtained in this experiment are not affected by such small changes in the rotational population.

Based on this assumption, we express the relative rovibrational population $p_{vJ}(t)=N_{vJ}(t)/\Sigma_{vJ}N_{vJ}(t)$ as

$$p_{vJ}(t)=p_v(t)p_J, \tag{13}$$

where $p_v(t)$ describes the total relative population of the vibrational level v and

$$p_J=\frac{(2J+1)e^{-J(J+1)B/kT}}{\sum_J (2J+1)e^{-J(J+1)B/kT}}. \tag{14}$$

This definition allows us to take into account the effect of a thermal rotational excitation on the kinetic energy release E_k.

Another aspect with regard to the rotational excitation of the ions is the dependence of the DR rate coefficient $\alpha_{vJnn'}(E)$ on the initial J quantum number. While a J dependence of the DR cross section exists in principle, its effect for relatively low J values is expected to be much smaller as compared to the effect of the v dependence [37,38]. Thus, to the extent of the present experiment, we have assumed a negligible rotational dependence of the rate coefficient, considering the dependence on the initial state to occur only through the vibrational quantum number v:

$$\alpha_{vJnn'}(E)\equiv\alpha_{vnn'}(E) \quad \text{for all } J. \tag{15}$$

Based on Eqs. (11) and (12), this implies that

$$q^{(E)}_{vJnn'}(t)=p_J q^{(E)}_{vnn'}(t) \tag{16}$$

and

$$r^{(E)}_{vJnn'}(t)=p_J r^{(E)}_{vnn'}(t). \tag{17}$$

Using Eqs. (10) and (16), the total projected distance spectrum is thus expressed by

$$P^{(E)}(D;t)=\sum_{vnn'} q^{(E)}_{vnn'}(t)\sum_J p_J P^{(E)}_{vJnn'}(D), \tag{18}$$

where $q^{(E)}_{vnn'}(t)$ describes the size of the contribution of the channel vnn' (summed over all J levels) to the projected distance spectrum, while the spectral shape of this contribution is given by Eq. (9) for the different rovibrational energy levels according to Eq. (6) after averaging over the thermal rotational level populations.

Relative DR rate coefficients for the state-to-state channels vnn' were extracted by fitting the spectrum $P^{(E)}(D;t)$ measured at time t with suitably fixed values for the kinetic energy releases $E_{k,vJnn'}$ entering Eq. (9), varying the weights $q^{(E)}_{vnn'}(t)$ and also the rotational temperature T. Regarding Eqs. (11)–(17), using the relative vibrational populations measured by Coulomb explosion imaging as described in Sec. II C, and taking the rate coefficient $\alpha_{021}(E)$ for $v=0$, $n=2$, and $n'=1$ as a reference, the relative rate coefficients were then obtained as

$$\frac{\alpha_{vnn'}(E)}{\alpha_{021}(E)}=\frac{q_{vnn'}(t)}{q_{021}(t)}\frac{p_0(t)}{p_v(t)}. \tag{19}$$

Note that, while both the relative contributions to the DR rate and the relative populations are time-dependent, their combinations according to Eq. (19) have to yield time-independent results.

2. Time-dependent vibration-averaged DR rate coefficients

In the preceding subsection, it was shown that it is possible to obtain the relative DR rate coefficients for a specific vibrational state using the two-dimensional imaging technique. Although such a technique is general, it can become extremely complicated once many final channels nn' are open, because of the difficulty in analyzing the imaging data. This is in particular the case at higher relative energies E between electrons and ions. Complications with regards to the DR fragment imaging technique then also arise because the fragmentation angle θ with respect to the ion beam axis [see the discussion preceding Eq. (9)] may no longer be isotropically distributed, as can be assumed for $E=0$.

Provided the relative populations of the different vibrational levels as a function of the storage time are markedly different from each other, it is also possible to obtain state-specific rate coefficients from the time dependence of the total number of DR events. The main difference is that in this case the final states of the DR process are unknown, so that the rate coefficient $\alpha_v(E)$ obtained by this method refers to a specific initial vibrational state v summed over all energetically possible final states for a given electron energy E.

The measured DR rate coefficient as a function of storage time t, $\alpha(t;E)$, is a sum over all the population-weighted specific rate coefficients from each vibrational state v:

$$\alpha(t;E)=\sum_v p_v(t)\alpha_v(E). \tag{20}$$

The state-specific rate coefficients $\alpha_v(E)$ can be extracted from a fit to the values of the vibration-averaged DR rate coefficient $\alpha(t;E)$ measured (at a given energy E) for a large sample of storage times t; the independently determined vibrational populations $p_v(t)$ are inserted in Eq. (20) and the set of rate coefficients $\alpha_v(E)$ is taken for the free parameters.

For the measurement of $\alpha(t;E)$, the neutral fragments H and D were detected by a 40×60-mm^2 energy-sensitive Si surface-barrier detector, replacing the two-dimensional imaging detector and being large enough to cover the full dissociation cones. The DR events were recorded requiring the full beam energy E_i to be deposited, corresponding to the simultaneous arrival of H and D on the detector. Small background contributions to this signal entered due to electron capture from the residual-gas atoms or molecules, leading to either bound neutral HD molecules or two neutral fragments H and D. Beside full beam energy events, also events of 2/3 and 1/3 of the beam energy were recorded, corresponding to a single D or a single H atom, respectively. These single neutral particles originated from the dissociation of the molecular ions HD^+ to $H + D^+$ or to $H^+ + D$, for which only the neutral fragment reached the detector. At low electron

energies, such dissociation events occur only due to collisions with the residual-gas particles in the straight section ahead of the detector. Once the energy of the free electron is above the dissociation energy of HD^+ (2.67 eV), molecular dissociation also originates from dissociative excitation (DE) of HD^+ by the electrons of the electron cooler.

The measurements were performed by recording the count rate at the full-energy peak of the Si detector $r^s(t;E)$ as a function of storage time t for various relative electron energies E. Both signal and background were determined by switching the electron acceleration voltage back and forth (at a rate of 30 Hz) between the level corresponding to E [where $r^s(t;E)$ was measured] and a very low value where the electron current and hence the electron-related count rate are negligible; the count rates $r^b(t)$ measured at this latter level were only due to background contributions. The background-subtracted DR rate $r(t)$ is given by

$$r(t;E)=r^s(t;E)-r^b(t), \tag{21}$$

from which the vibration-averaged DR rate coefficient $\alpha(t;E)$ can be deduced as

$$\alpha(t;E)=r(t;E)/\eta n_e(E)N(t). \tag{22}$$

Here $n_e(E)$ is the electron density at the electron energy E, $N(t)$ is the total number of ions in the ring at time t, and $\eta=L/C$ is the ratio between the length of the interaction region ($L=1.5$ m) and the ring circumference ($C=55.4$ m). The electron density $n_e(E)$ was extracted from the electron current measured at the collector of the electron cooler. Usually, the number $N(t)$ of stored ions is deduced from the ion current circulating in the ring as it is measured by the current transformer of the TSR. However, in the present experiment the current was too low for such measurement. Thus no absolute measurement of the number of ions was possible, and absolute rate coefficients could not be extracted. In order to obtain a signal proportional to the ion beam current, apart from an overall normalization factor, previous measurements on vibrationally relaxed ions used the background count rates of single neutral fragments produced in the residual gas, r_H^b and r_D^b. In the present measurement with vibrationally relaxing ions, such a procedure might be wrong since the single fragment production in residual gas collisions could be sensitive also to the vibrational excitation of the molecular ions. Thus, a quantity which is proportional to $N(t)$ was obtained from another procedure.

For every injection, the average background rate of single neutral fragments, $r_H^b(t_{rel})+r_D^b(t_{rel})$, was recorded after complete vibrational relaxation in a storage time interval centered at $t_{rel}=450$ ms (specifically, the interval of 400–500 ms). In a separate step under the same experimental conditions, but with the ion beam bunched by a radiofrequency cavity, an electrical signal $S(t)$ proportional to the number of HD^+ ions in the ring could be observed on a pickup electrode near the ion beam. The relatively weak signal was averaged over many injections and yielded the relative time dependence of the circulating ion current, which was used to derive, from the rate of background events measured after each injection for a relaxed beam, the number of ions at any storage time t,

$$N(t)=G[r_H^b(t_{rel})+r_D^b(t_{rel})][S(t)/S(t_{rel})], \tag{23}$$

where G is an overall normalization constant independent of the vibrational excitation of the ion beam.

In summary, to derive the state-specific rate coefficients from the time dependence of the total DR rate, first the vibration-averaged rate coefficients $\alpha(t;E)$ are deduced using Eqs. (21])–(23), and then Eq. (20) and the vibrational populations $p_v(t)$ are applied to extract the rate coefficient for each vibrational level v. Since in the present experiment G is unknown, the state-specific DR rate coefficients are obtained in arbitrary units.

C. Vibrational population measurement

1. Basic measurement

The vibrational population distribution of the ion beam circulating in the TSR was measured by probing a small fraction of the beam, continuously extracted from the ring using a slow spill technique. The relative populations of vibrational states in these extracted ions were sampled using the Coulomb explosion imaging (CEI) technique. Details about the CEI method and the experimental setup at the TSR, including the extraction part, can be found elsewhere [39–41], and only a short description will be given here.

In a CEI experiment [39], a beam of fast molecular ions collides with a very thin (<100 Å thick) solid target so that all binding electrons are rapidly stripped. For MeV beams, such stripping occurs on a time scale of $\sim 10^{-16}$ s, i.e., much shorter than the typical vibrational ($>10^{-14}$ s) or rotational ($>10^{-12}$ s) times. Moreover, the full dwell time in the foil of $\sim 10^{-15}$ s is much smaller than the characteristic time scale of the Coulomb explosion dynamics, so that the nuclear motion is basically unaffected by the foil, except for a small smearing effect resulting from the multiple scattering of the nuclei with the target atoms. The exiting fragments then ''Coulomb explode'' due to the strong repulsion between the ion cores, converting their potential energy into kinetic energy in the center-of-mass frame of reference. A few hundred Å from the foil surface, most of the initial Coulomb energy has been transformed into kinetic energy and the fragments reach their asymptotic velocities. The asymptotic kinetic energy ($\tilde{E}_k$) of the fragments in their center-of-mass frame of reference can be determined experimentally at a distance $\tilde{s}$ of a few meters from the foil using a three-dimensional imaging technique, which measures the relative two-dimensional distance $\tilde{D}$ on the plane of the detector (perpendicular to the beam direction) and the relative time of arrival Δt between the molecular fragments:

$$\tilde{E}_k=\frac{E_i}{\tilde{s}^2}\frac{m_H m_D}{(m_H+m_D)^2}[(v_i\Delta t)^2+\tilde{D}^2], \tag{24}$$

where v_i is the ion beam velocity. The $\tilde{E}_k$ distribution measured for an ensemble of ions can be used to extract their initial internuclear distance (R) distribution before stripping, which is directly related to the square of the nuclear wave function. As such, the $\tilde{E}_k$ distribution is sensitive to the initial vibrational population distribution [40].

In the present experimental setup [41], HD^+ ions extracted from the TSR were collimated by two apertures of 2 mm diam situated 3 m apart (see Fig. 2) before hitting a formvar target of a measured 70-Å thickness. The imaging detector (*A* in Fig. 2) was situated at a distance of $\tilde{s} = 2965$ mm from the target and is basically composed of an ion-electron conversion foil producing an electron shower for each ion impact, a two-stage MCP, and a phosphor screen together with a set of anode strips (see Ref. [41] for details). The two-dimensional distance $\tilde{D}$ was deduced in the same way as for the two-dimensional imaging of the DR fragments described in Sec. II B 1, i.e., using a CCD camera which digitized the images of the light spots created on the phosphor screen, and was coupled to a fast frame grabber device read out by a computer. The difference Δt between the arrival times of the fragments was obtained using timing signals from the anode strips located behind the phosphor screen. A resolution of ~ 100 ps (FWHM) was obtained for the timing of a single fragment. On analysis, the spatial and the timing data were correlated to yield simultaneously the relative distance $\tilde{D}$ and the time interval Δt between the impacts for each pair of H^+ and D^+ fragments. Using a beam chopper in front of the stripping foil, the CEI measurements were performed molecule by molecule.

2. Evaluation of vibrational populations

The evaluation of vibrational populations is based on the characteristic shapes of kinetic energy distributions for Coulomb explosion of molecules in different vibrational states v. Based on the predicted shape $P_v^{\tilde{E}_k}(\tilde{E}_k)$ of such energy distributions, the relative populations $p_v(t)$ $[\Sigma_v p_v(t) \equiv 1]$ are determined by fitting to the experimental data the superposition

$$P^{\tilde{E}_k}(\tilde{E}_k;t) = \sum_v p_v(t) P_v^{\tilde{E}_k}(\tilde{E}_k), \tag{25}$$

where $P_v^{\tilde{E}_k}(\tilde{E}_k)$ is the normalized kinetic energy distribution for an ensemble of ions in a given vibrational state v.

In a simplified, semiclassical description of the Coulomb explosion process, the kinetic energy distribution $P_v^{\tilde{E}_k}(\tilde{E}_k)$ is directly related to the initial internuclear distance distribution $P_v^R(R)$ according to

$$P_v^{\tilde{E}_k}(\tilde{E}_k) d\tilde{E}_k = P_v^R(R) dR = \Psi_v^2(R) dR, \tag{26}$$

where the kinetic energy release $\tilde{E}_k$ as a function of the internuclear distance is given by the Coulomb law; for HD^+,

$$\tilde{E}_k(R) = e^2/R. \tag{27}$$

The distribution $P_v^R(R)$ is identical to the square of the nuclear wave function $\Psi_v(R)$ for the vibrational state v. Note that in this approximation it is also assumed that the nuclei are at rest in the center-of-mass frame of reference before the collision with the target.

To obtain sufficiently accurate predictions for the kinetic energy distributions associated with the different vibrational states, several small but non-negligible modifications have to be applied to the above simplified description. Firstly, the multiple scattering and charge exchange that the molecular fragments undergo in the foil have to be accounted for. Second, Eq. (27) neglects the initial momentum of the bound nuclei prior to Coulomb explosion. However, this initial momentum leads to an additional contribution to $\tilde{E}_k$ becoming important for high vibrationally excited states, where the initial kinetic energy of the fragments represents 10–15 % of the total kinetic energy release (1–2 eV as compared to an average Coulomb potential energy of ~ 13.5 eV). The correct inclusion of the initial momentum of the fragments requires a quantum-mechanical treatment of the Coulomb explosion process. As a third modification, the finite resolution of the imaging detector must be accounted for.

The first and the last of the required modifications can be applied by using an existing classical Monte-Carlo simulation of the molecular Coulomb explosion starting with random initial conditions (i.e., internuclear distances R) as given by the squared nuclear wave function. Details about this simulation can be found in a previous publication [42]. It computes the classical trajectories of the dissociating fragments including all known effects related to MeV molecule-solid interaction and dissociation dynamics, and also includes the detector resolution in deriving the kinetic energy distributions $P_v^{\tilde{E}_k}(\tilde{E}_k)$. Its reliability has been proven in various earlier experiments, where the main focus was on molecular structure for lower vibrational states. The correction for foil effects and detector resolution typically amounts to a broadening of the energy distribution by about 20% and is fully taken into account by the simulation so that these effects do not affect the retrieval of the vibrational population.

This approach does not account for the initial momentum distribution of the nuclei. It is straightforward in principle to calculate quantum mechanically the $\tilde{E}_k$ distribution, including the effect of the initial momentum distribution, by projecting the bound-state wave function onto continuum wave functions of given energies $\tilde{E}_k$. However, such calculation does not include the target effects and the experimental energy resolution as discussed above. In order to combine all the corrections, the following approximate procedure was applied for each individual vibrational state:

(a) In a first step, the quantum-mechanical distribution $Q_v^{\tilde{E}_k}(\tilde{E}_k)$ of the asymptotic kinetic energy $\tilde{E}_k$ of the fragments in their center-of-mass frame of reference was obtained, assuming a pure Coulomb explosion without any experimental effects due to the foil or the detector. The initial nuclear wave function was projected on a basis set composed of Coulomb wave functions $\chi_c(R;k,J)$, each characterized by the wave number $k = \hbar^{-1}[2\tilde{E}_k m_H m_D/(m_H + m_D)]^{1/2}$ and the conserved (in the stripping process) angular momentum J. The kinetic energy distribution $Q_{vJ}^{\tilde{E}_k}(\tilde{E}_k)$, corresponding to the initial state vJ, is obtained according to

$$Q_{vJ}^{\tilde{E}_k}(\tilde{E}_k) d\tilde{E}_k = Q_{vJ}^k(k) dk = |C_{vJ}^k|^2 \, dk, \tag{28}$$

with

$$C_{vJ}^k = \int \chi_c^*(R;k,J) \Psi_{vJ}(R) dR. \tag{29}$$

In the present experiment, our ensemble of ions was at a rotational temperature of a few hundred degrees K, hence only low values of J are of interest. For different low J values with the same k value, the calculations of C^k_{vJ} yielded similar results which are not distinguishable experimentally. Thus, for simplicity, $J=0$ was assumed throughout the calculation, and the final result for the kinetic energy distribution is given by

$$Q_v^{\tilde{E}_k}(\tilde{E}_k)d\tilde{E}_k=|C^k_{vJ=0}|^2\,dk. \tag{30}$$

The function $Q_v^{\tilde{E}_k}(\tilde{E}_k)$ represents the exact kinetic energy release distribution for the dissociation of a molecular ion through the pure Coulomb potential.

(b) In order to include the foil effects and the effects of the finite detector resolution, the quantum-mechanical Coulomb explosion was inverted assuming classical trajectories in the pure Coulomb potential. Using the relation $Q_v^{\tilde{E}_k}(\tilde{E}_k)d\tilde{E}_k=Q_v^R(R)dR$ in connection with Eq. (27), that (artificial) R distribution $Q_v^R(R)$ was calculated which, for classical trajectories, yields the quantum-mechanical distribution $Q_v^{\tilde{E}_k}(\tilde{E}_k)$.

(c) This artificial R distribution $Q_v^R(R)$ was then used as the initial R distribution for the Monte-Carlo simulation, yielding the final function $P_v^{\tilde{E}_k}(\tilde{E}_k)$ for fitting the experimental $\tilde{E}_k$ distributions.

Using the set of distributions $P_v^{\tilde{E}_k}(\tilde{E}_k)$ obtained from this procedure, the experimental data $P^{\tilde{E}_k}(\tilde{E}_k;t)$ were fitted taking the relative populations $p_v(t)$ of the different vibrational levels as free parameters.

III. RESULTS

A. Vibrational population distribution

1. Time evolution

To analyze the vibrational distribution of the stored HD^+ ions as a function of the storage time, spectra of the kinetic energy release $\tilde{E}_k$ after Coulomb explosion were measured for injection cycles repeated at intervals of 1 s. Examples of spectra showing the vibrational relaxation are shown in Fig. 3 for four storage time slices (i.e., various vibrational population distributions). After 400 ms, the kinetic energy distribution is found to be time-independent.

Qualitatively, the vibrational cooling of the HD^+ molecular ions is exhibited through two time-dependent features of the CEI spectra: on one hand, the spectrum is getting narrower with time, and on the other hand, its peak is shifting toward higher kinetic energy values. For short times the kinetic energy distribution is very wide as a result of the broad distribution of vibrational states populated on injection; the higher the vibrational excitation v, the wider its vibrational wave function and the corresponding kinetic energy distribution $P_v^{\tilde{E}_k}(\tilde{E}_k)$ [see Eqs. (26) and (27)]. The shift in the peak is expected as a result of the anharmonicity of the HD^+ molecular potential for the high-lying vibrational states populated. Initially, the molecule has a higher probability to be found at larger internuclear distances R, corresponding to lower final kinetic energies $\tilde{E}_k$.

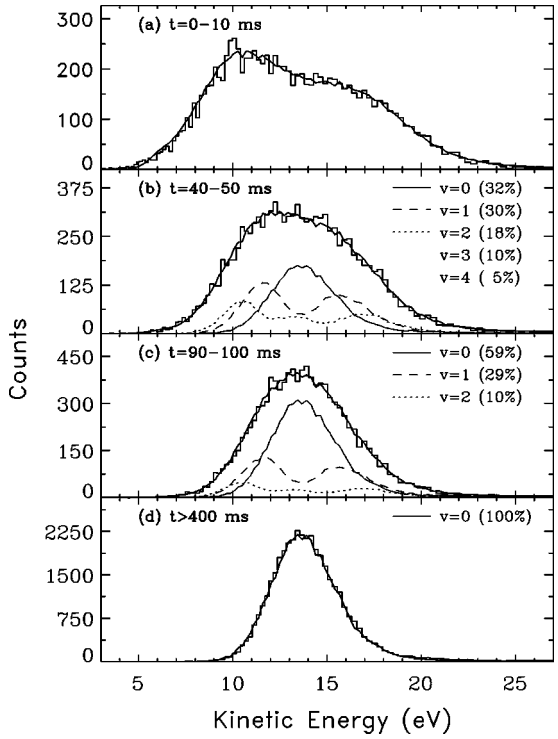

FIG. 3. Kinetic energy spectra measured for Coulomb explosion imaging of HD^+ for different storage time slices: (a) 0–10 ms, (b) 40–50 ms, (c) 90–100 ms, and (d) $t>400$ ms. The thick solid lines represent the fits as described in the text. Panels (b)–(d) display also the vibrational populations (those above 5%) obtained from the fit, together with the main contributions to the spectrum (thin solid, dashed, and dotted lines).

Quantitatively, following the procedure described above in Sec. II C 2, the kinetic energy spectrum $P^{\tilde{E}_k}(\tilde{E}_k;t)$ for each time slice was fitted using the calculated spectra $P_v^{\tilde{E}_k}(\tilde{E}_k)$ for each of the different v levels of HD^+ with the relative populations $p_v(t)$ as free parameters. The nuclear vibrational wave functions $\Psi_v(R)$ needed for the calculations were computed by solving the Schrödinger equation for the known ground electronic potential curve of HD^+ [43]. A direct and simple comparison can be made with the spectrum shown in Fig. 3(d), which is the kinetic energy distribution for the ground state of HD^+ after relaxation of the stored ions. The distribution $P_{v=0}^{\tilde{E}_k}(\tilde{E}_k)$ calculated for ground-vibrational-state HD^+ molecular ions is shown as a smooth solid line on top of the measured data in Fig. 3(d), demonstrating a very good mutual agreement. This particular comparison is also important for the fine tuning of parameters entering the Monte-Carlo simulation described in Sec. II C 2, mainly the target foil thickness. As these parameters are constant for all vibrational states, they were optimized to provide the best possible fit to the coldest measured spectrum.

The results of the fit for the experimental distributions in Figs. 3(a)–3(c) are shown as smooth solid lines on top of the experimental data. Note that the calculated curves include noise originating from the Monte-Carlo simulation. Also indicated are the main partial contributions to the spectrum and the resulting vibrational populations (above 5%).

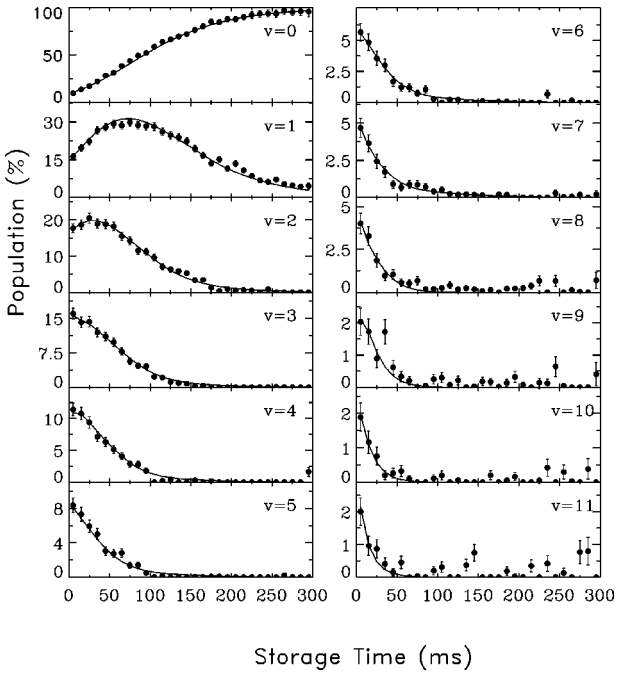

FIG. 4. Time evolution of the vibrational-state population $p_v(t)$ for $0 \leqslant v \leqslant 11$, normalized to $\Sigma_v p_v(t) = 100\%$, as obtained from fitting the time-sliced CEI kinetic energy spectra, of which some examples are given in Fig. 3. The smooth lines through the experimental points are the results of fitting the time evolution of the measured populations by the theoretical model as described in the text.

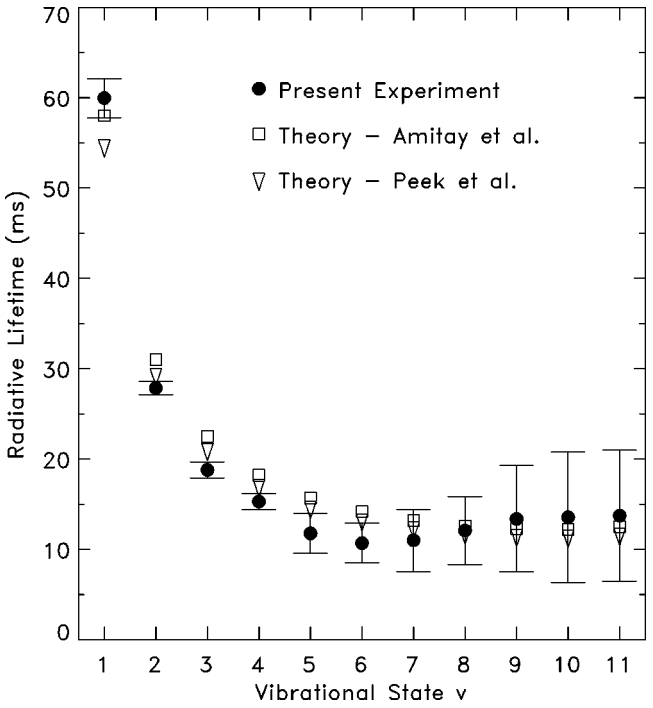

FIG. 5. The values of the radiative lifetime for various vibrational levels of HD^+, as obtained from fitting the time evolution of the populations given in Fig. 4 (see text). Together with the experimental values are shown two sets of theoretical results calculated by Amitay *et al.* [21] (open squares) and by Peek *et al.* [46] (open triangles).

Figure 4 summarizes the time evolution of the derived populations $p_v(t)$ for the vibrational states $v = 0$–11 over storage times t ranging from 0 to 300 ms in 10-ms bins, normalized to $\Sigma_v p_v(t) = 100\%$. The population of $v = 0$ is rising with time from $\sim 10\%$ at injection to 100% after 400 ms, while the vibrational states $v = 1$ and 2 exhibit an initial rise in their population, followed by a decrease when the deexcitation to lower vibrational states overcomes the feeding from the upper vibrational levels. In the following subsection, we compare the time dependence of the vibrational populations to a simple theoretical model.

2. Radiative lifetimes and initial populations

For HD^+, as for any infrared active molecular ion, the time evolution of the vibrational populations $p_v(t)$ during the storage in the ring is completely determined by the initial populations of the vibrational states upon production and injection, $p_v(0)$, and by the radiative lifetimes τ_v of the different levels.

The recursive rate equations describing the time evolution for each level v are of the form

$$\frac{dp_v(t)}{dt} = -\frac{1}{\tau_v} p_v(t) + \frac{1}{\tau_{v+1}} p_{v+1}(t). \tag{31}$$

If the initial population for levels above $v_{\max}$ is assumed to be negligible [i.e., $p_v(0) = 0$ for $v > v_{\max}$], the general solution of the set of rate equations is

$$p_v(t) = a_{vv} e^{-t/\tau_v} + \sum_{v'=v+1}^{v_{\max}} a_{vv'} e^{-t/\tau_{v'}} + b_v, \tag{32}$$

where $a_{vv'}$ and b_v are time-independent constants. Inserting this general solution into the set of rate equations of Eq. (31) and assuming $\tau_v \neq \tau_{v+1}$ (a correct assumption for HD^+), one gets for the constants $a_{vv'}$ the iterative expression

$$\begin{aligned} a_{vv} &= p_v(0) - \sum_{v'=v+1}^{v_{\max}} a_{vv'} \quad \text{for } 0 \leqslant v \leqslant v_{\max}, \\ a_{vv'} &= \frac{a_{v+1,v'}}{\tau_{v+1}(1/\tau_v - 1/\tau_{v'})} \quad \text{for } v+1 \leqslant v' \leqslant v_{\max}, \end{aligned} \tag{33}$$

and $b_v = 0$.

The observed time-dependent vibrational populations shown in Fig. 4 were fitted using the analytical solution for $v_{\max} = 11$ with the radiative lifetimes τ_v and the initial populations $p_v(0)$ as free parameters, yielding the smooth lines in Fig. 4. Figures 5 and 6 show the fit results for the radiative lifetimes and for the initial populations of the various vibrational levels, respectively. The large errors for the higher vibrational levels, especially for $v = 9$–11, are due to their very small initial populations, which make their relative contributions to the CEI data difficult to extract precisely.

Together with the experimental results for the radiative lifetimes, Fig. 5 presents theoretical values calculated by Amitay *et al.* [21] and by Peek *et al.* [46]. The calculations by Amitay *et al.* were carried out for various rotational levels

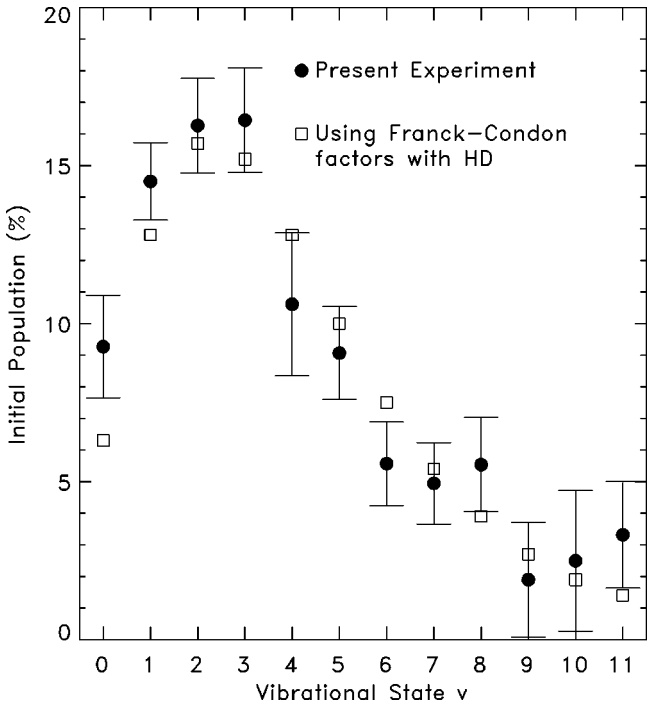

FIG. 6. The initial (normalized) vibrational population distribution (upon production and injection into the ring), as obtained from fitting the time evolution of the populations given in Fig. 4 (see text). Also shown are results of calculations which assumed production of HD^+ by direct electron impact ionization of HD, yielding vibrational populations according to the Franck-Condon factors between the wave functions of the ground-state HD and the different vibrational states of HD^+.

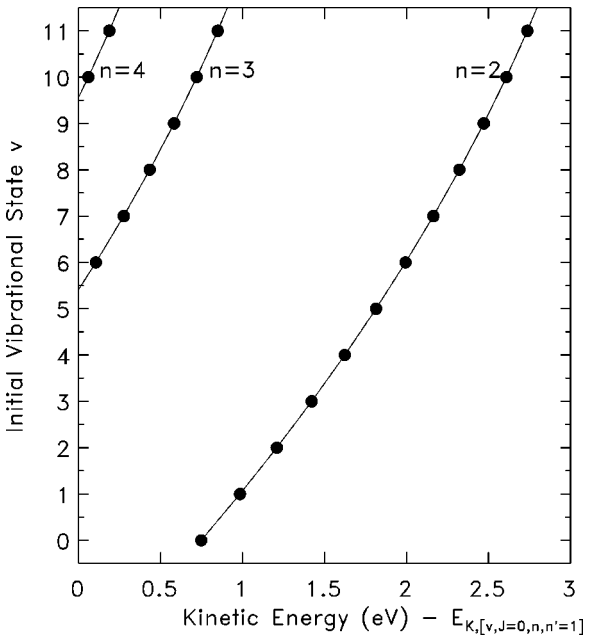

FIG. 7. Calculated kinetic energy release for the DR of HD^+ with zero energy electrons as a function of the initial vibrational state v for various final states $n=2$, 3, and 4. The lines are drawn to guide the eyes.

up to $J=7$, yielding lifetimes which vary over the different J levels of a specific vibrational level by up to $\sim 20\%$, becoming shorter for higher rotational excitation. The values shown here (open squares) were calculated for $J=3$, the average J value of the experimental rotational distribution corresponding to a few hundred up to ~ 1000 K. The calculations by Peek *et al.* were done for $J=0$. The general trends of the experimental and the theoretical results are consistent with each other, and although the experiment yields systematically slightly smaller lifetime values for $2 \leqslant v \leqslant 7$ and a slightly higher value for $v=1$, a good overall agreement is obtained. To our knowledge, this is the first direct measurement for the lifetimes of the vibrational states of HD^+, and as such, the results can be used as a benchmark for future calculations.

The resulting values for the initial vibrational populations $p_v(0)$, shown in Fig. 6, exhibit a distribution peaked between $v=2$ and 3. They are compared to the populations calculated with the assumption that the electron impact ionization in the ion source can be described by vertical direct transitions from the electronic and vibrational ground state of HD to the electronic ground state of HD^+, thus yielding populations according to the Franck-Condon factors of the different vibrational states of HD^+ with the ground state of HD. For most of the vibrational levels these predictions lie within the experimental error bars; disagreement beyond the experimental error only exists for $v=0$, where the theory underestimates the initial population. Deviations of the experimental results from this simple prediction may be related to the fact that the calculation did not take into account the variation of the electronic matrix elements for direct electron-impact ionization with the internuclear separation. An attempt to perform such a calculation was done by Von Busch and Dunn [35] in order to analyze the photodissociation cross section of H_2^+. Moreover, deviations might be caused by the additional production of HD^+ by excitation of HD to Rydberg states and following by autoionization. The autoionization of singly excited HD Rydberg states requires a conversion of internal vibrational energy to electronic energy and hence vibrational deexcitation of the ionic (HD^+) core. Thus, assuming the electronic excitation of Rydberg states to leave the ionic core with similar vibrational populations as the direct electron-impact ionization, the final vibrational populations of HD^+ after autoionization are likely to be shifted to lower excitation. Indeed, the comparison between the experimental and the calculated populations indicates a slight trend to lower excitation. A similar explanation was also given by Von Busch and Dunn [35]. Finally, the electron impact processes in the ion source can also lead to electronically doubly excited states of HD which can autoionize by direct electronic interaction. These processes would again be expected to yield different vibrational populations from direct ionization.

Altogether, the degree of consistency found between the experimental results and theoretical predictions, both for the radiative lifetimes and the initial vibrational populations, strongly confirms the reliability of the time-dependent vibrational populations of the stored ions as measured by the CEI technique.

B. State-to-state DR rate coefficients at $E=0$

In this subsection, we present the results for the vibrational-state specific DR rate coefficients of HD^+ ob-

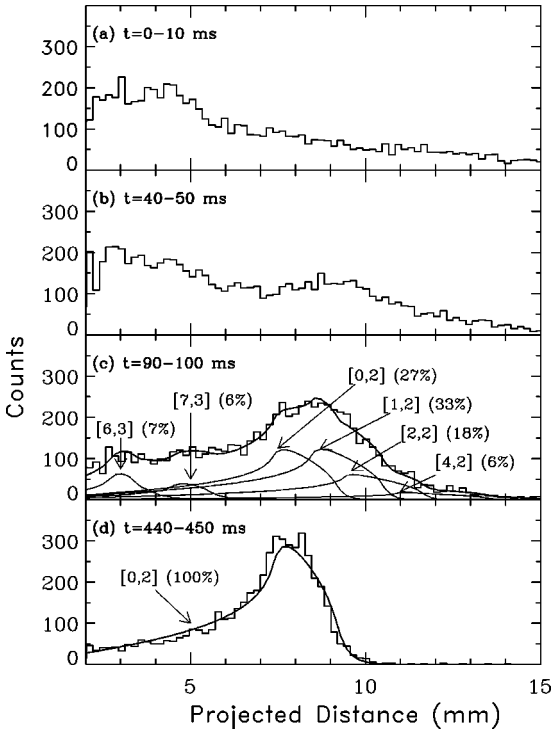

FIG. 8. Projected distance distributions as measured between the H and D fragments from the DR of vibrationally excited HD^+ at matched electron and ion beam velocities ($E=0$) at different storage times: (a) 0–10 ms, (b) 40–50 ms, (c) 90–100 ms, and (d) 440–450 ms. On top of the data in panels (c) and (d) are drawn (in solid lines) the overall fits of the measured distributions. Panel (c) also shows individual contributions $[v,n]$ from DR starting at the vibrational level v and ending at the final asymptote of given n with $n'=1$ (see text).

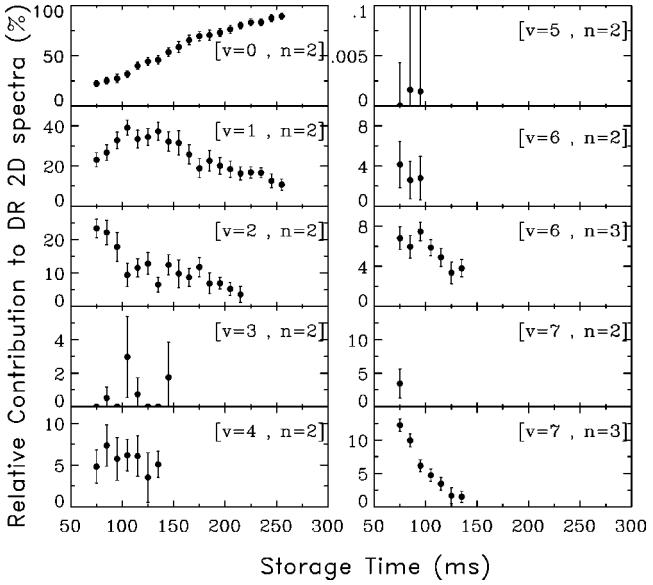

FIG. 9. Fitting results for the relative contribution from each initial-to-final state-to-state DR channel $[v,n]$ to the projected-distance distribution measured at $E=0$ at different storage times t. $[v,n]$ stands for DR starting at the vibrational level v and ending at the final asymptote of given n with $n'=1$ (see text).

tained by the two-dimensional imaging technique at matched average velocities of electron and ion beam ($E=0$). At the corresponding low collision energies, and assuming the rotational excitation to be restricted to $J<10$, only the final asymptotes with one of the H and D fragments in the states $n=1$ or 2 are accessible through DR as long as $v<5$. The next set of final states, $n=3$, can energetically be reached only from $v=5$ if $J\geqslant 5$, or from $v\geqslant 6$. The other fragment always stays in the ground state ($n'=1$); the asymptotes for which both fragments are excited become accessible only at collision energies above 12 eV, which are not applied in this experiment. Figure 7 shows for an electron energy $E=0$ the relation between the kinetic energy release $E^{(E=0)}_{k,v,J=0,n,n'=1}$ and the initial vibrational excitation of HD^+, considering the asymptotes $n=2$–4. From projecting the plotted points onto the kinetic energy axis it is clear that (at least up to $v=9$) each value of $E^{(E=0)}_{k,v0n1}$ is sufficiently separated from neighboring points to uniquely identify both the initial v and the final n state of the DR process. At higher excitation additional asymptotic states are open; however, in the present work only $v=0$–7 will be considered, as the experimentally derived populations of the higher states ($v\geqslant 8$) have too large uncertainties to be useful (see Fig. 4).

Figures 8(a)–8(d) show some of the observed projected-distance spectra measured for the DR of HD^+, using the 2D imaging technique described in Sec. II B 1, as a function of the storage time (i.e., sampling different vibrational population distributions). Here again, for storage times longer than 400 ms, the projected-distance distribution is constant, since the molecular ions are fully relaxed and no more changes in the vibrational population distribution take place.

Qualitatively, the time evolution of the projected-distance spectrum is characterized by a rapid change either at large or small projected-distance regions. These regions of the distance spectrum correspond mainly to either very high or very low kinetic energy, respectively. At long storage time, the obtained distribution is concentrated mainly at intermediate projected distances [Fig. 8(d)], and is the one which is expected for DR starting from $v=0$ and ending at $n=2$ [solid smooth line in Fig. 8(d)]. The other final asymptote $n=1$, which is also energetically accessible from $v=0$, is not populated, as was already demonstrated in a previous experiment [22]. At shorter storage times and correspondingly high vibrational excitation, contributions at large projected distances are mainly due to DR events originating from $v>0$ vibrational states and ending at the $n=2$ asymptote. In addition, contributions at small projected distance are observed, which result mainly from DR events ending at the $n\geqslant 3$ channels, accessible essentially for $v\geqslant 6$ and leading to small kinetic energy release according to Fig. 7. Many such channels are open for the high initial vibrational excitation of the ion beam.

The analysis of the projected-distance spectra was carried out following the procedure described in Sec. II B 1. For each measured time-sliced projected-distance spectrum $P^{(E=0)}(D;t)$, the distribution was fitted using the function described by Eq. (18) with the rotational temperature T and the various contributions to the spectrum, $q^{(E=0)}_{vnn'}(t)$, as free parameters. The solid line shown on top of the data in Fig. 8(c) results from such a fit. Several individual contributions to the spectra are also shown. As can be seen, these functions are well-separated, yielding contributions in characteristic ranges of projected distance, so that their relative contribu-

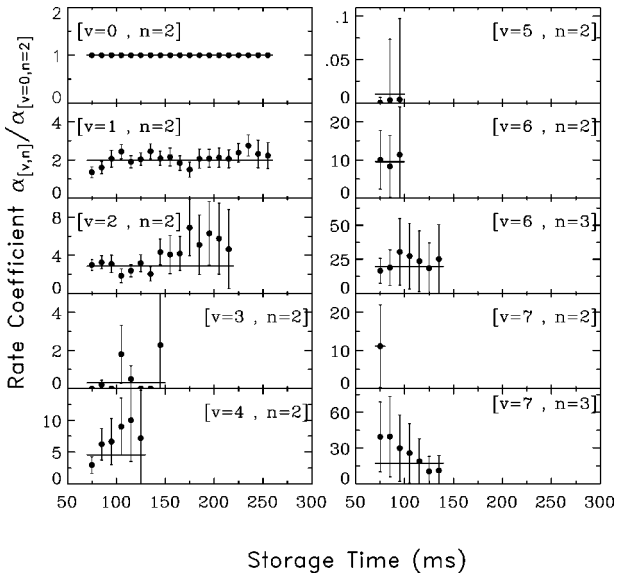

FIG. 10. Relative DR rate coefficients at $E=0$ for the various initial-to-final state-to-state DR channels as a function of storage time. The straight lines represent the average values used as the final result.

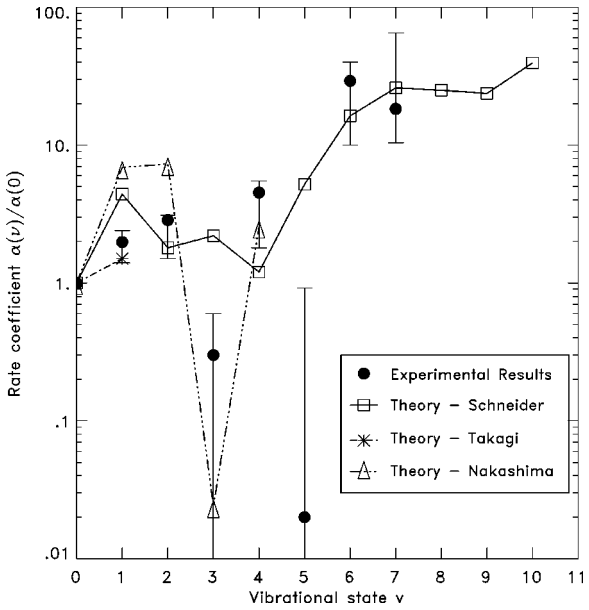

FIG. 11. Final experimental results for the relative DR rate coefficients of HD^+ at $E=0$ as a function of the initial vibrational quantum number. Except for $v=5$, where the result is only for dissociation to the $n=2$ asymptote, the displayed values have been summed over all possible final states. Together with the experimental results are also shown the theoretical calculations by Schneider and Suzor for $v=0-10$ [30], by Takagi for $v=0$ and 1 [44], and by Nakashima *et al.* for $v=0-4$ [18]. Both experiment and theories are normalized to unity for $v=0$. The lines through the theoretical results are drawn to illustrate the trends of the results from the various calculations.

tions can be extracted. Figure 9 summarizes the fit results for the relative contributions $q^{(E=0)}_{vnn'}(t)/\Sigma_{vnn'}q^{(E=0)}_{vnn'}(t)$ of each initial-to-final state-to-state DR channel to the projected-distance distribution measured at the different storage times t. The values obtained for the rotational temperature were also varied in the single fits and found to be in the range $T=450-750$ K, consistent with the expected initial rotational population in the ion source and only a small degree of rotational cooling. Projected-distance spectra for storage times of <70 ms and correspondingly very high vibrational excitation were not included in these results, as the many superimposed contributions could no longer be identified in an unambiguous way. It is important to point out that, since only projected distances above 2 mm could reliably be measured by the 2D imaging detection system, contributions from DR with very low kinetic energy release could not be quantified and are also not included in the sum used for normalizing the results of Fig. 9. However, for our restricted range of $v=0-7$, this only excludes the contributions from $v=5$, $J\geqslant 5$, to the final asymptote $n=3$.

In the further analysis, the various DR signal contributions $q^{(E=0)}_{vnn'}(t)$ and the measured vibrational populations $p_v(t)$ (see Sec. III A 2) were used to derive the state-to-state DR rate coefficients $\alpha_{vn1}(0)$ relative to that of $v=0$, $n=2$, $n'=1$, denoted $\alpha_{021}(0)$, i.e., $\alpha_{vn1}(0)/\alpha_{021}(0)$ [see Eq. (19)]. Figure 10 presents the results obtained for various time slices. Within their errors bars the values are time independent as required. This fact strongly underlines the reliability of the method used to extract the rate coefficients. The errors of the relative rate coefficients in a single time slice are dominated by the uncertainties of the contributions $q^{(E=0)}_{vnn'}(t)$ to the projected-distance DR spectrum as long as the vibrational populations $p_v(t)$ remain above $\sim 2.5\%$. For increasing storage time, the populations of excited states gradually decrease and their uncertainties dominate the error in many cases, except when the relative contributions to DR are small (such as for $v=3,n=2$).

The final experimental results of the state-to-state relative DR rate coefficients were taken as the mean values over the different time slices. They are shown in Fig. 10 as straight lines. Figure 11 summarizes the final results as a function of the initial vibrational quantum state v. The value for each specific v level was obtained after summation over all energetically accessible final states n. The only exception is the value for $v=5$, where, as pointed out above, the $n=3$ channel (open for $v=5,J\geqslant 5$ only) produces events with too small projected distances. The experimental results shown in Fig. 11 agree within the error bars with the ones published earlier [30]; however, the time-dependent vibrational populations were taken in the present case from the fitted curves obtained by varying both the initial populations $p_v(0)$ and the vibrational lifetimes τ_v (see Sec. III A 2), while in the previous publication only the values of $p_v(0)$ were varied. The results of Fig. 11 and those shown in Fig. 4 of Ref. [30] are fully consistent with each other.

Together with the final experimental results, Fig. 11 shows theoretical calculations by Schneider and Suzor for $v=0-10$ (presented in Ref. [30]), as well as previous results by Takagi for $v=0-1$ [44] and by Nakashima *et al.* for $v=0-4$ [18]. All these calculations used variants of the multichannel quantum defect theory [16] with slightly different sets of molecular data. Takagi's calculations and those of Nakashima *et al.* have considered only the $^1\Sigma_g^+$ dissociative state of HD (see Fig. 1), while Schneider and Suzor's results

were obtained taking into account also the higher Q_1 dissociative states (see Fig. 1). It is important to point out that the results by Schneider and Suzor and by Takagi have been convoluted with the experimental (i.e., anisotropic) electron velocity distribution, while those by Nakashima *et al.* have been obtained for an isotropic Maxwell-Boltzmann distribution corresponding to 100 K. Only Takagi's calculations account for the effect of the rotational motion on the DR cross section, and his results are for a rotational temperature of 800 K. The two other calculations were done for $J=0$.

For the low vibrational states, a large spread exists among the different theoretical predictions as well as between these and the experimental results. In general, the calculations succeed to reproduce some but not all of the measured values. For example, the particularly low experimental value found for the relative rate coefficient of $v=3$ is reproduced only by the calculations of Nakashima *et al.* A very large discrepancy is found for $v=5$. It is important to point out that this difference cannot be related to the fact that contributions from the $v=5, J\geqslant 5$ states are not included in the experimental results (see above), as the calculations are done for $J=0$. The low value for $v=5$ could not be reproduced, even when the calculations by Schneider and Suzor [30] were repeated using different sets of calculated potential curves.

For the higher vibrational levels, the overall trend of the experimental results demonstrates that a considerably larger DR rate coefficient is obtained for $v>5$ as compared to those of $v<5$. This trend is qualitatively reproduced by the results of Schneider and Suzor. Moreover, the experimental relative rate coefficients of 10 to 55 for $v=6$ and 7 are also well reproduced quantitatively. Nevertheless, the strong increase of the recombination rate predicted theoretically already for $v=5$ is experimentally observed only for $v\geqslant 6$. Possible reasons for the differences between the theoretical predictions and the observed relative DR rate coefficients will be discussed in Sec. IV. subsection

Vibrational-state specific DR rate coefficients at $E=3-11$ eV

In this part of the experiment, vibrational-state specific rate coefficients were measured for the DR of HD^+ with $v=0-3$ as functions of the electron energy in the high energy range $E=3-11$ eV. The measurement was performed by following the total DR rate for a given electron energy E over storage times of the ions in the ring from 10 to 500 ms in 10-ms time-binning, as described in Sec. II B 2.

In the range of energies covered, the DR of HD^+ for low vibrational states is known to be due to the capture of an electron in the Q_1 states of HD** (see Fig. 1). Various measurements have shown that for $HD^+(v=0)$ ions a strong peak exists in the DR cross section at about 9 eV, whose shape reflects the initial shape of the nuclear wave function of the molecular ion [25,27]. Accordingly, for vibrationally excited molecules the cross section in this energy region should change strongly. A second peak in the cross section, smaller by a factor of ~ 2 and due to the Q_2 states of HD**, occurs near 16 eV for $v=0$ ions; its shape is similarly governed by that of the initial vibrational wave function but for not-too-high vibrational excitation the Q_2 states should influence the cross section only above ~ 12 eV.

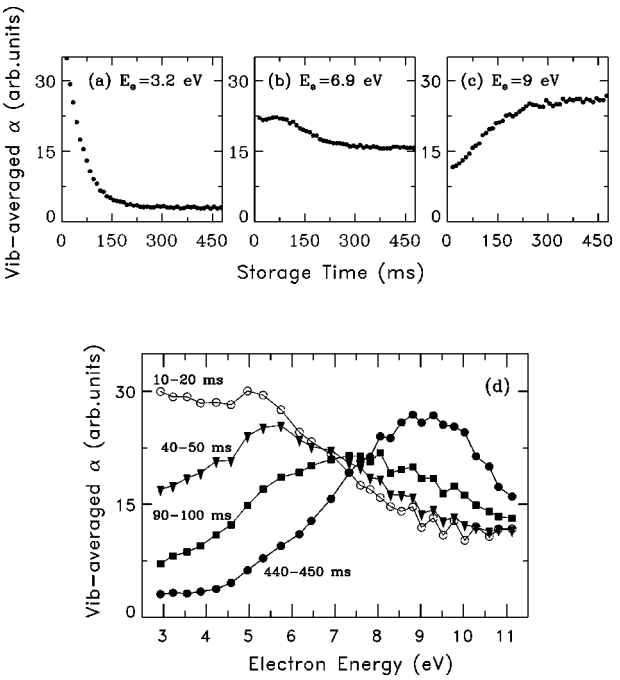

FIG. 12. Time dependence of the vibration-averaged DR rate coefficient measured with electron in the energy range 3–11 eV. Panels (a)–(c) show the measurement as a function of the storage time for three particular electron energies: (a) 3.2 eV, (b) 6.9 eV, and (c) 9 eV. Panel (d) shows the measurement as a function of the electron energy E for various particular time slices: 10–20 ms, 40–50 ms, 90–100 ms, and 440–450 ms.

Figures 12(a)–12(c) present the dependence on the storage time t of the vibration-averaged DR rate coefficient $\alpha(t;E)$ as measured at the electron energies of $E=3.2$, 6.9, and 9 eV, respectively. The DR rates were normalized to the total circulating ion current as described in Sec. II B 2 up to an arbitrary constant independent of electron energy and storage time. As can be seen, each of the measurements exhibits a different time evolution; however, all curves after ~ 400 ms approach a constant asymptotic value which corresponds to the DR rate coefficient of $v=0$ at the respective E. At 3.2 eV, $\alpha(t)$ exhibits a high value at short times followed by a very fast continuous decrease with time. The 6.9-eV spectrum displays a more complex structure with a small peak located at ~ 75 ms on top of a moderate decay, while the 9-eV data show a strong rise as a function of time.

Figure 12(d) shows the same measurements as a function of the electron energy for various time slices. As expected, for $t=440-450$ ms, when all ions are vibrationally relaxed, the rate coefficient exhibits the well-known peak near 9 eV [25–28]. For shorter times, the cross-section maximum moves to lower energy, indicating that for high vibrational states lower electron energies are sufficient to reach the Q_1 states in vertical transitions; see Fig. 1.

With the relative populations $p_v(t)$ obtained from the fit functions representing the time evolution of the populations measured by CEI, as described in Sec. III A 2, the values of $\alpha_v(E)$ were extracted using Eq. (20). The four coefficients $\alpha_v(E)$ with $v=0-3$ were fitted to the measured time-dependent function $\alpha(t;E)$ for each E at times $t\geqslant 80$ ms. In this time range vibrational states $v>3$ are already very weakly populated and should yield a negligible contribution to the total DR rate. For the states $v=2$ and 3, only the sum

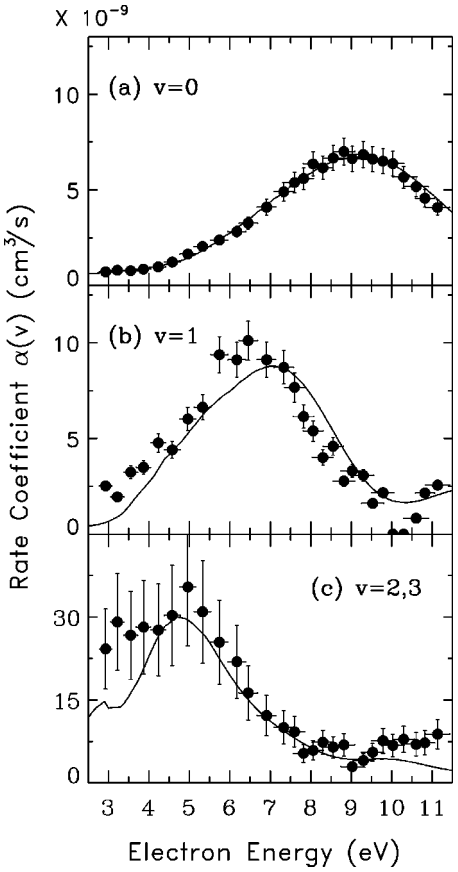

FIG. 13. State-specific DR rate coefficients of $HD^+(v)$ (experimental results normalized to reproduce the peak of the calculated rate coefficient for $v=0$) in the energy region of 3–11 eV for $v=0$–3. For $v=2$ and 3, only the sum of their rate coefficients is shown (see the text). The solid lines are the results of MQDT calculations including competition with dissociative ionization.

of the fitted coefficients is given, since the time evolutions $p_v(t)$ of both state populations are very similar to each other as soon as $t \geqslant 50$ ms and consequently a strong correlation occurs between $\alpha_2(E)$ and $\alpha_3(E)$. The results of $\alpha_2(E)+\alpha_3(E)$ might contain systematic, energy-dependent errors due to this procedure, since the ratio $p_2(t)/p_3(t)$ is not exactly constant for all t. Figures 13(a)–13(c) present these results as a function of the electron energy E. All results contain a common unknown normalization constant which was set to fit the theoretical rate coefficient by Schneider and Suzor at energies around 9 eV for $v=0$. The theoretical results of these authors are shown by solid lines in Fig. 13.

The results shown in Figs. 13(a)–13(c) demonstrate that the resonance structure, which for $v=0$ peaks at ~ 9 eV, is shifted to lower energies for higher v values, with a peak at ~ 6.7 eV for $v=1$ and at ~ 5 eV for the summed $v=2$ and 3 rate coefficients. The peak heights clearly increase with v. In view of these state-specific results, one can reexamine the time evolutions of $\alpha(t;E)$ presented in Figs. 12(a)–12(c). At $E=3.2$ eV, the fast and steady decrease is due to deexcitation of the high vibrational states populated initially; at $E=6.9$ eV, the small temporal maximum at 75 ms closely follows the time evolution of the $v=1$ population; finally, at $E=9$ eV the entire time evolution of the measured rate coefficient is basically governed by that of the $v=0$ population.

The bending regions of the electron beam near the ends of its strictly collinear overlap section with the ion beam yield additional contributions to the measured recombination rates at a given energy, stemming from recombination at higher electron energies which are reached in the bending regions [23]. In particular, the measured recombination rates on the low-energy sides of peaks with widths of a few eV for our geometry contain contributions from the bending regions of $\sim 7\%$ of the peak value, which, for example, could account for the complete rate observed at 3–4 eV for relaxed ions [$t=440$–450 ms, see Fig. 12(d)]. If the DR rate coefficient over a large range of higher electron energies is known, the effect of the bending regions can be deconvoluted from the data [23]; however, the necessary information is not available at all storage times, and hence such a deconvolution was not applied for the present results. This slightly restricts the extent to which a detailed comparison can be performed between the experimental results and the theoretical calculations. In particular, the $v=0$ DR rate at 3–6 eV may in fact be overestimated by the theory in spite of the detailed agreement apparent from Fig. 13(a). Nevertheless, it is found that the theory reproduces both the shift of the peak in the cross section and the relative peak height for the various vibrational states rather well.

IV. DISCUSSION

A. Low-energy region

At low electron energy ($E=0$), and for the first five vibrational states $v=0$–4, the relative rate coefficients measured for the DR of $HD^+(v)$ show a large variation (see Fig. 11), and no specific trend can be observed. Such variations over the different v levels are probably due to the different Franck-Condon factors between the initial vibrational wave function and the dissociative wave function of the $^1\Sigma_g^+$ state that is the dominant route of DR for these levels. The $^1\Sigma_g^+$ state crosses all the vibrational levels of HD^+, except for $v=0$, in the oscillating region of their wave function. Since the various Franck-Condon factors are expected to be very sensitive to the exact location of the crossing, they can vary from one level to another by sometimes more than an order of magnitude. For example, the low experimental value observed for $v=3$ is reproduced by the calculations of Nakashima *et al.* [18], who explicitly attribute their low result for this state to a very small Franck-Condon factor. The large spread among the theoretical calculations might then originate from the slightly different $^1\Sigma_g^+$ potential curves used in each of them. However, it is important to point out that also more complex effects might be involved, such as a variation of the autoionization width with the internuclear distance along the dissociative $^1\Sigma_g^+$ potential curve. These effects can be clearly observed, for example, for the ratio of the rate coefficients between $v=1$ and $v=0$. While the measured ratio is 2 (see Fig. 11), the ratio between the Franck-Condon factors is about 10. Thus, although a simple argument based on Franck-Condon factors may lead to a qualitative understanding of the changes, it does not allow us to quantify the ratio of the rate coefficients directly.

For high vibrational excitations ($v>5$), the overall trend that the rate coefficients increase relative to their values at lower v levels is explained by an opening of new and very efficient dissociation routes through the Q_1 dissociative states lying above the $^1\Sigma_g^+$ state. This behavior is well reproduced by the calculations of Schneider and Suzor [30]. The particularly low experimental value found for $v=5$ can also, in principle, be explained by low Franck-Condon factors with both the $^1\Sigma_g^+$ state and the higher Q_1 states, and the failure of the theory to reproduce this low value might again be attributed to errors in the potential curves used by the calculations. However, the fact that the calculations by Schneider and Suzor could not reproduce the result even when they were repeated with different sets of potential curves seems to weaken this argument [30].

Another possible explanation is that these calculations, while in fact obtaining a correct cross section for the initial electron capture and also the correct factor describing the stabilization against autoionization at *short* internuclear distances, did not give a full account of the long-range internuclear dynamics. According to the calculations, the dominant dissociating curve for $v=5$ is the lowest Q_1 state above $^1\Sigma_g^+$, which has $^3\Pi_g$ symmetry, while for $v=0-4$ the most important state is the $^1\Sigma_g^+$ state itself. The $^3\Pi_g$ curve diabatically dissociates to the $n=2$ asymptote of the H and D fragments; thus, disregarding possible dynamics at large internuclear distances, the whole dissociating flux would be ending up via the $^3\Pi_g$ state at this asymptote, still the only one energetically open for at least the low-J states of $v=5$. The calculations were actually conducted under this assumption, due to insufficient knowledge of the electronic interactions at large distances. However, considering the avoided crossings between the $^1\Sigma_g^+$ state and the Rydberg series, it is highly probable that, during the dissociation, part of the flux will be redirected toward the still closed $n=3$ asymptote, but then reflected back to short internuclear distances where it can be lost via autoionization. A strong transfer of flux to states correlating to the still closed $n=3$ channel could thus explain the observed reduction of the recombination rate for this particular vibrational level. Clearly, such a hypothesis needs more theoretical calculations to be verified.

For $v=6$ and 7, where the experimental results are reproduced successfully, this explanation is not relevant as in these cases the $n=3$ asymptote is already open. For these two states, it was indeed found that the $n=3$ asymptote is the dominant one (see Fig. 10), an evidence supporting the above arguments to explain the low rate coefficient measured for $v=5$. Yet, it can be claimed that the dynamics at large internuclear distances should be of high complexity and very sensitive to the total energy of the system, thus varying from one vibrational level to another. More full-scale calculations are needed to clarify this point.

B. High-energy region

The state-selective DR rate coefficients measured in the energy region $E=3-11$ eV for $v=0-3$ were found to be in good agreement with theory. In this energy region, DR occurs mainly through the doubly excited Q_1 states of HD. Here, the direct DR mechanism controls the process, and the obtained rate coefficients depend directly on the Franck-Condon factors between the initial bound vibrational wave function and the continuum wave functions in the various active dissociative curves of HD. Accordingly, the energy dependences of the DR cross sections (or rate coefficients) can be largely understood by considering the shapes of the various ground-state or excited vibrational HD^+ wave functions. It is interesting to note that also the relative strengths of the recombination rate coefficients for $v=0-3$ are well reproduced by the theory. Note also that these calculations take account of the dissociative ionization, a competitive process to DR at high energy [27]. Based on this overall good agreement, it seems that the high energy DR of HD^+ is now well understood, except for the angular anisotropy, which was discovered a few years ago [22].

V. CONCLUSIONS

The DR of HD^+ in specific vibrational states has been measured using a technique based on probing the time-dependent vibrational population of a beam circulating in an ion storage ring by Coulomb explosion imaging (CEI). The advantage of this technique is that no initial state preparation is needed and, in general, rate coefficients can be extracted for all the states significantly populated in the ion source. The HD^+ molecular ions used here cool in a relatively short period of time; however, such rapid changes in population are convenient but not necessary, and the basic method can also be used for molecular ions without a dipole moment, such as H_2^+. The main disadvantage of the technique is its lack of sensitivity for rotational excitation, and the fact that it requires relatively high energy beams in order to perform clean CEI experiments.

State-specific cross sections can be extracted in a similar way for other processes on molecular ions, such as dissociative excitation, photodissociation, or, for negative molecular ions, photodetachment or electron impact neutralization.

ACKNOWLEDGMENTS

This work was funded in part by the German Federal Minister for Education, Science, Research and Technology (BMBF) under Contract No. 06 HD 854 I, the EU/HCM program, by the German Israel Foundation (GIF) under Contract No. I-0452-200.07/95, and by the German Federal Minister of Education, Science, Research and Technology (BMBF) within the framework of the German-Israeli Project Cooperation in Future-Oriented Topics (DIP).

[1] J. N. Bardsley, J. Phys. B **1**, 349 (1968); **1**, 365 (1968).

[2] *Dissociative Recombination: Theory, Experiment and Applications*, edited by J. B. A. Mitchell and S. L. Guberman (World Scientific, Singapore, 1989), and references therein.

[3] D. R. Bates and H. S. W. Massey, Proc. R. Soc. London, Ser. A **192**, 1 (1947).

[4] D. Kella *et al.*, Science **276**, 1530 (1997), and references therein.

[5] S. L. Guberman, Science **278**, 1276 (1997), and references therein.

[6] M. B. McElroy, M. J. Prather, and J. M. Rodriguez, Science **215**, 1614 (1982).
[7] M. B. McElroy, Science **175**, 443 (1972); J. L. Fox, Geophys. Res. Lett. **20**, 1747 (1993); M. H. G. Zhang *et al.*, J. Geophys. Res., [Space Phys.] **98**, 10 915 (1993).
[8] J. L. Fox, in *Dissociative Recombination: Theory, Experiment and Applications*, edited by J. B. A. Mitchell and S. L. Guberman (World Scientific, Singapore, 1989), p. 264, and references therein.
[9] J. L. Fox, in *Dissociative Recombination: Theory, Experiment and Applications*, edited by B. R. Rowe, J. B. A. Mitchell, and A. Canosa (Plenum Press, New York, 1993), p. 219, and references therein.
[10] D. Kella *et al.*, Phys. Rev. Lett. **77**, 2432 (1996), and references therein.
[11] L. H. Andersen *et al.*, Phys. Rev. Lett. **77**, 4891 (1996), and references therein.
[12] S. L. Guberman, Nature (London) **327**, 408 (1987).
[13] S. L. Guberman, *Dissociative Recombination: Theory, Experiment and Applications*, edited by J. B. A. Mitchell and S. L. Guberman (World Scientific, Singapore, 1989), p. 45.
[14] S. L. Guberman and A. Giusti-Suzor, J. Chem. Phys. **95**, 2602 (1991).
[15] J. H. Yee, V. J. Abreu, and W. B. Colwell, in *Dissociative Recombination: Theory, Experiment and Applications*, edited by J. B. A. Mitchell and S. L. Guberman (World Scientific, Singapore, 1989), p. 286.
[16] A. Giusti-Suzor, J. Phys. B **13**, 3867 (1980).
[17] A. Giusti-Suzor, J. N. Bardsley, and C. Derkits, Phys. Rev. A **28**, 682 (1983).
[18] K. Nakashima, H. Takagi, and H. Nakamura, J. Chem. Phys. **86**, 726 (1987).
[19] M. Larsson, Annu. Rev. Phys. Chem. **48**, 151 (1997), and references therein.
[20] U. Hechtfischer *et al.*, Phys. Rev. Lett. **80**, 2809 (1998).
[21] Z. Amitay, D. Zajfman, and P. Forck, Phys. Rev. A **50**, 2304 (1994).
[22] D. Zajfman *et al.*, Phys. Rev. Lett. **75**, 814 (1995).
[23] Z. Amitay *et al.*, Phys. Rev. A **54**, 4032 (1996).
[24] D. Zajfman *et al.*, Phys. Rev. Lett. **79**, 1829 (1997).
[25] P. Forck *et al.*, Phys. Rev. Lett. **70**, 426 (1993).
[26] T. Tanabe *et al.*, Phys. Rev. Lett. **75**, 1066 (1995).
[27] C. Strömholm *et al.*, Phys. Rev. A **52**, R4320 (1995).
[28] L. H. Andersen *et al.*, Phys. Rev. A **55**, 2799 (1997).
[29] W. J. van der Zande *et al.*, Phys. Rev. A **54**, 5010 (1996).
[30] Z. Amitay *et al.*, Science **281**, 75 (1998).
[31] B. W. Shore *et al.*, Phys. Rev. A **45**, 5297 (1992).
[32] D. Habs *et al.*, Nucl. Instrum. Methods Phys. Res. B **43**, 390 (1989).
[33] S. L. Guberman, J. Chem. Phys. **78**, 1404 (1983).
[34] H. Helm and P. C. Cosby, J. Chem. Phys. **86**, 6813 (1987).
[35] F. Von Busch and G. H. Dunn, Phys. Rev. A **5**, 1726 (1972).
[36] G. Herzberg, *Spectra of Diatomic Molecules* (Van Nostrand, New York, 1979).
[37] H. Takagi, J. Phys. B **26**, 4815 (1993).
[38] I. F. Schneider *et al.*, J. Phys. B **30**, 2687 (1997).
[39] Z. Vager, R. Naaman, and E. P. Kanter, Science **244**, 426 (1989).
[40] D. Zajfman, Comments At. Mol. Phys. **29**, 369 (1994).
[41] R. Wester *et al.*, Nucl. Instrum. Methods Phys. Res. A **413**, 379 (1998).
[42] D. Zajfman, T. Graber, E. P. Kanter, and Z. Vager, Phys. Rev. A **46**, 194 (1992).
[43] T. E. Sharp, At. Data **2**, 119 (1971).
[44] H. Takagi, in *Dissociative Recombination: Theory, Experiment and Applications III*, edited by D. Zajfman, J. B. A. Mitchell, D. Schwalm, and B. R. Rowe (World Scientific, Singapore, 1996), p. 174.
[45] M. Tadjeddine and G. Parlant, Mol. Phys. **33**, 1797 (1977).
[46] J. M. Peek, A. R. Hashemi-Attar, and C. L. Beckel, J. Chem. Phys. **71**, 5382 (1979).